

Macroporous Catalytic Carbon Nanotemplates for Sodium Metal Anodes

Hyeon Ji Yoon, Na Rae Kim, Hyoung-Joon Jin,* and Young Soo Yun*

Because of its remarkably high theoretical capacity and favorable redox voltage (-2.71 V vs the standard hydrogen electrode), Na is a promising anode material for Na ion batteries. In this study, macroporous catalytic carbon nanotemplates (MC-CNTs) based on nanoweb-structured carbon nanofibers with various carbon microstructures are prepared from microbe-derived cellulose via simple heating at 800 or 2400 °C. MC-CNTs prepared at 800 °C have amorphous carbon structures with numerous topological defects, and exhibit a lower voltage overpotential of ≈ 8 mV in galvanostatic charge/discharge testing. In addition, MC-CNT-800s exhibit high Coulombic efficiencies of 99.4 – 99.9% during consecutive cycling at current densities ranging from 0.2 to 4 mA cm $^{-2}$. However, the carbon structures of MC-CNTs prepared at 800 °C are gradually damaged by cycling. This results in significant capacity losses after about 200 cycles. In contrast, MC-CNTs prepared at 2400 °C exhibit well-developed graphitic structures, and maintain predominantly stable cycling behaviors over 1000 cycles with Coulombic efficiencies of $\approx 99.9\%$. This study demonstrates the superiority of catalytic carbon nanotemplates with well-defined pore structures and graphitic microstructures for use in Na metal anodes.


With tremendous growth in modern electronic devices and the advent of a knowledge-based economy, there is a significant interest in developing high-performance energy storage devices based on practical technologies.^[1–3] While conventional rechargeable battery systems composed of two host electrodes that operate via intercalation of charges are improving, they have intrinsic energy and power limitations because of their limited equivalent charge storage sites.^[4,5] Although host structure-free materials based on conversion and alloying reactions sometimes exhibit theoretical capacities several times larger than those of intercalation compounds, they also suffer from several major issues such as large voltage hysteresis, irreversible capacities, unfavorable voltage characteristics, insufficient

Coulombic efficiencies, and poor cycling stabilities. They are barely suitable as active materials for current needs.^[6–14] Lithium and sodium metal have recently been proposed as alternative negative electrode materials because of their low redox potentials (-3.04 and -2.71 V vs the standard hydrogen electrode, respectively) and high theoretical capacities (3860 and 1166 mA h g $^{-1}$, respectively) which are 10 and 3 times higher, respectively, than that (372 mA h g $^{-1}$) of a graphite anode in a typical Li ion battery.^[15,16] Nevertheless, these metal anodes have fatal problems such as low Coulombic efficiencies, infinite volume changes, and unpredictable metal electrodeposition (dendritic growth), which lead to capacity decay, cycling limitations, and safety hazards caused by the repeated electrochemical dissolution and deposition of metal.^[17–23] To address these issues, several efforts have been made to introduce additives into electrolytes,^[24–30] carbon-based templates,^[31–36] or protective coating layers.^[37–40] In particular, Zheng et al. reported a sophisticated electrode design with an interconnected hollow carbon nanosphere cover layer that allows a uniform Li ion flux at the electrode level, which leads to stability over 150 cycles.^[34] Zhang et al. proposed a unique channel structure to provide a pathway that guides the Li deposition/dissolution process. It effectively mitigates electrode volume changes and alleviates the dendritic growth of Li metal.^[35] In addition, a glyme-based electrolyte can suppress dendritic growth while improving the Coulombic efficiency without use of an additive or additional Na metal anode processing.^[41–44] These results suggest that introducing a carbon-based catalytic template and glyme-based electrolyte can alleviate the major shortcomings of metal anodes. Furthermore, nanostructured design of the template structure may provide significantly more active sites for metal deposition and dissolution. This can induce a uniform Na ion flux throughout the electrode, leading to high rate capabilities and stable cycling via obstruction of dendritic metal growth at high charge/discharge rates.

In this study, we designed macroporous catalytic carbon nanotemplates (MC-CNTs) composed of hierarchically interconnected carbon nanofibers with various local microstructures synthesized from microbe-derived cellulose via simple heating at temperatures from 800 to 2400 °C. Carbon-based MC-CNT monoliths $1/2$ in. in diameter were used as anode materials without metal substrates and binders. MC-CNT-800 and

H. J. Yoon, N. R. Kim, Prof. H.-J. Jin
Department of Polymer Science and Engineering
Inha University
Incheon 402-751, South Korea
E-mail: hjjin@inha.ac.kr

Prof. Y. S. Yun
Department of Chemical Engineering
Kangwon National University
Samcheok 245-711, South Korea
E-mail: ysyun@kangwon.ac.kr

 The ORCID identification number(s) for the author(s) of this article can be found under <https://doi.org/10.1002/aenm.201701261>.

DOI: 10.1002/aenm.201701261

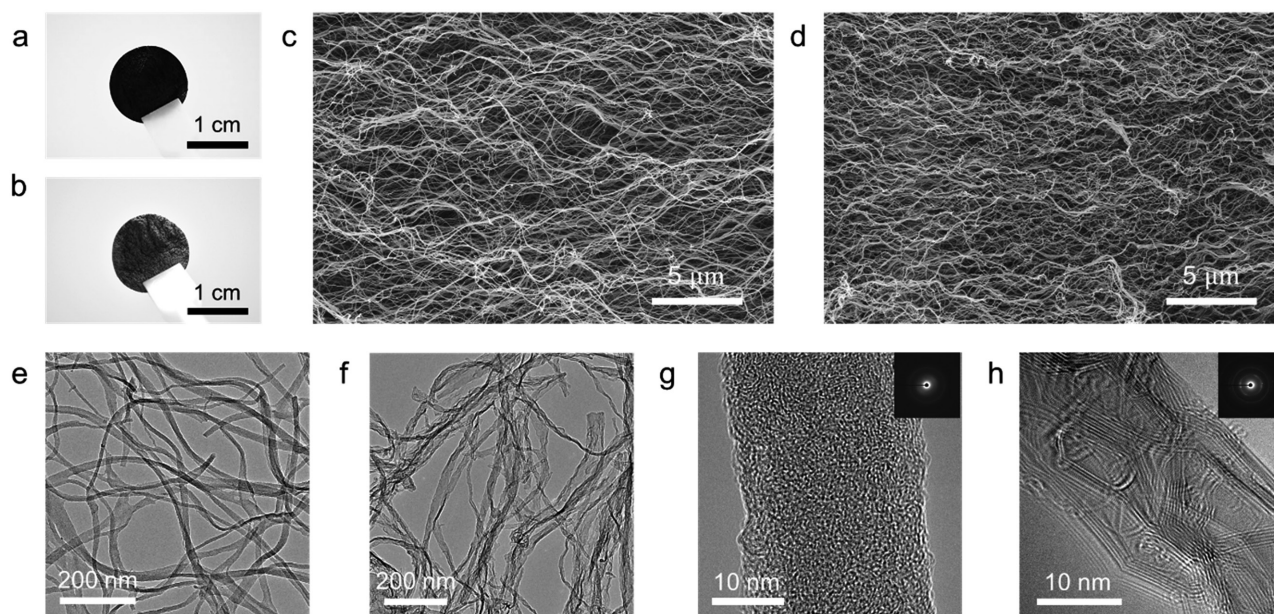


Figure 1. Characterization of the morphologies of MC-CNT-800 and MC-CNT-2400. a,b) Optical, c,d) FE-SEM, and e,f) FE-TEM images of MC-CNT-800 and MC-CNT-2400, respectively. High-resolution FE-TEM images of g) MC-CNT-800 and h) MC-CNT-2400 with (inset) the selected area diffraction patterns.

MC-CNT-2400 (where the heat-treatment temperature is indicated at the end of the sample name, e.g., -800, -2400) exhibited overpotentials of ≈ 8 and 10 mV, respectively, at $50 \mu\text{A cm}^{-2}$. This is significantly lower than that of bare Al foil (≈ 25 mV), as becomes clear at increasing current densities, indicating more active sites. In addition, MC-CNT-800 and MC-CNT-2400 exhibit high Coulombic efficiencies of 99.9% at a current density of 1 mA cm^{-2} (1 A g^{-1}). Above all, MC-CNT-2400 maintains stable cycling behavior with a Coulombic efficiency of 99.9% over 1000 cycles, in contrast to the limited cycling stability (≈ 200 cycles) of MC-CNT-800. Ex situ characterization was used to help understand the origin of the superior cycling performance of MC-CNT-2400.

Optical imaging shows MC-CNT-800 and MC-CNT-2400 monoliths that are black and graphite-like gray, respectively. The gray color of MC-CNT-2400 suggests that it possesses a well-developed graphitic structure (Figure 1a,b). The morphologies of MC-CNT-800 and MC-CNT-2400 were further examined via field emission scanning electron microscopy (FE-SEM), as shown in Figure 1c,d, as well as Figures S1 and S2 (Supporting Information). Macroporous nanoweb structures composed of entangled carbon nanofibers $\approx 20\text{--}30$ nm in diameter and several micrometers in length (aspect ratio >100) are confirmed. The carbon nanofibers in the network structure of MC-CNT-2400 are thinner and denser than those of MC-CNT-800. This is thought to be because of thermal shrinkage of $\approx 30\%$ during graphitization (Figure 1c,d). Field emission transmission electron microscopy (FE-TEM) images also show the nanoweb structures of the MC-CNT samples (Figure 1e,f). High-resolution FE-TEM images further reveal their microstructural differences (Figure 1g,h). While MC-CNT-800 has an amorphous carbon structure without long-range carbon ordering, MC-CNT-2400 possesses a distinctive graphitic structure (Figure 1g,h). Selected area electron diffraction patterns also support this

claim (Figure 1g,h, insets). Further microstructural characterization was performed using Raman spectroscopy and X-ray diffraction (XRD). The Raman spectrum of MC-CNT-2400 shows clear D and G bands centered at ≈ 1350 and 1580 cm^{-1} , respectively (Figure 2a). The D band corresponds to the disordered A_{1g} breathing mode of the hexagonal carbon structure, while the G band originates in the six-membered aromatic ring and is related to the E_{2g} vibration mode of the sp^2 hybridized C atoms.^[45] The presence of narrow and fully separate D and G bands indicates a well-developed hexagonal carbon structure. In addition, a large 2D band centered at $\approx 2677 \text{ cm}^{-1}$ is observed in the Raman spectrum of MC-CNT-2400. This indicates 3D stacking and ordering of its hexagonal carbon structures.^[45] A clear graphitic (002) peak at 26.1° in the XRD pattern of MC-CNT-2400 supports the Raman results (Figure 2b). In contrast, the Raman spectrum of MC-CNT-800 shows relatively broad, fused D and G bands centered at ≈ 1332 and $\approx 1581 \text{ cm}^{-1}$, respectively. This indicates more defective, smaller, hexagonal carbon structures. Furthermore, there is no 2D band in this spectrum, which indicates that the structures within it exhibit no 3D carbon ordering. The XRD pattern of MC-CNT-800 supports this result via a very broad graphitic (002) peak at $\approx 25^\circ$ that suggests poor graphitic ordering. Gradual changes in the carbon microstructures of MC-CNT samples as a function of their heat-treatment temperatures ($800\text{--}2400^\circ\text{C}$) are confirmed by Figure S3 (Supporting Information).

The pore structures of MC-CNT-800 and MC-CNT-2400 were analyzed via nitrogen adsorption and desorption isotherm curves, as shown in Figure 2c. The overall shapes of the isotherms are similar, and the quantity of nitrogen adsorbed increases dramatically above a relative pressure of 0.8, indicating the presence of macroporous structures.^[46] This result is corroborated by the FE-SEM images. The specific surface areas of MC-CNT-800 and MC-CNT-2400 are 101 and $104 \text{ m}^2 \text{ g}^{-1}$,

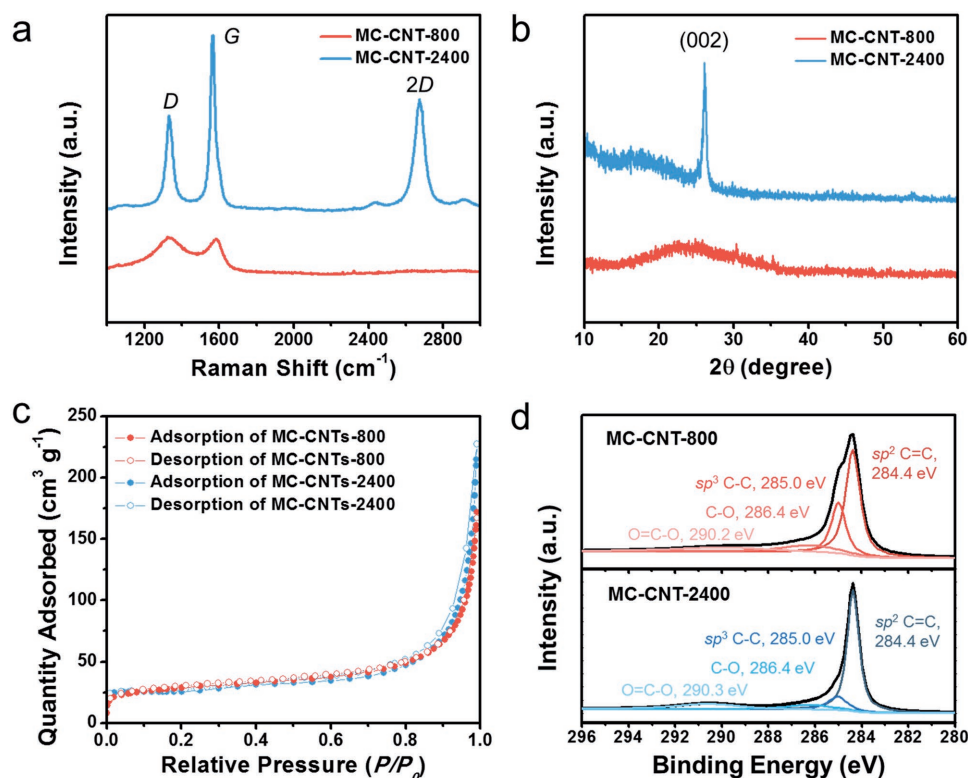


Figure 2. Material properties of MC-CNT-800 and MC-CNT-2400. a) Raman spectra, b) XRD patterns, c) nitrogen adsorption and desorption isotherms, and d) XPS C 1s spectra of the two materials.

respectively, which are ≈ 1000 times higher than that of bare Al foil. The surface properties of MC-CNT-800 and MC-CNT-2400 were investigated via X-ray photoelectron spectroscopy (XPS), as shown in Figure 2d. A sharp sp^2 C=C bonding peak centered at 284.4 eV is observed in the C 1s spectrum of MC-CNT-2400 alongside minor sp^3 C-C, C-O, and O=C-O bonding peaks centered at 285.0, 286.4, and 290.2 eV, respectively. The C 1s spectrum of MC-CNT-800 exhibits a large sp^3 C-C bonding peak centered at 285.0 eV, unlike MC-CNT-2400. The major sp^2 C=C bonding peak centered at 284.4 eV and minor C-O and O=C-O bonding peaks centered at 286.4 and 290.3 eV, respectively, from MC-CNT-800 are similar to those of MC-CNT-2400.^[47,48] The C/O ratios of MC-CNT-800 and MC-CNT-2400 are 28.8 and 114.0, respectively, and suggest that the quantities of oxygen present are insignificant. The XPS survey spectrum can be found in Figure S4 (Supporting Information).

Cyclical galvanostatic plating and stripping of sodium metal on MC-CNT-800 and MC-CNT-2400 were performed in 1 M NaPF₆ dissolved in diethylene glycol dimethyl ether (DEGDME) without additives, with a cut-off capacity of 500 mA h g⁻¹. Areal loading densities of 1 mg cm⁻² were used with both MC-CNT samples, and bare Al foil was tested as a control. The superiority of glyme-based electrolytes compared with carbonate-based electrolytes was confirmed by ex situ FE-SEM characterizations (see Figure S5 of the Supporting Information). The early sections of the voltage profiles of the working electrodes measured at a current density of 50 μ A cm⁻² show sodium plating in both electrode systems (Figure 3a). And voltage overshooting is observed when sodium deposition begins. This may

be due to a nucleation barrier of electrochemically deposited metal.^[33,49] In addition, an initial capacity gap is observed between MC-CNT-800 and MC-CNT-2400 before voltage overshooting occurs. The capacity gap may originate from chemisorption or insertion of sodium ions in the different carbon microstructures.^[50] The Al foil electrode exhibits a higher overpotential (around ≈ 25 mV) than MC-CNT-800 or MC-CNT-2400 (≈ 7 and ≈ 9 mV, respectively) at a low current density of 50 μ A cm⁻². This indicates that the MC-CNT samples exhibit more quantitative and/or qualitative catalytic active sites than Al foil. The voltage overpotential of the other MC-CNT samples was also characterized, and is shown in Figure S6 (Supporting Information). Topological and edge defects, pseudo-edge sites, and heteroatoms on hexagonal carbon structures may act as catalytic sites for sodium plating.^[51] Therefore, since the carbon structure of MC-CNT-800 is more defective than that of MC-CNT-2400 and the other MC-CNT samples, MC-CNT-800 is expected to be superior for the catalytic effects. However, despite their large microstructural differences, the overpotential gap between the two MC-CNT samples is small. Thus, a qualitative and quantitative study is required. Although the recursive relationship between carbon defects and their catalytic effects is interesting, it is outside the scope of our study. We can confirm that MC-CNT-800 shows the least overpotential of the samples tested. The Coulombic efficiencies of the electrodes were further tested at various current densities via continuous galvanostatic plating/stripping cycles, as shown in Figure 3b. MC-CNT-800 and MC-CNT-2400 exhibit excellent Coulombic efficiencies of 99.4–99.9% and 99.5–99.9%, respectively, at current densities

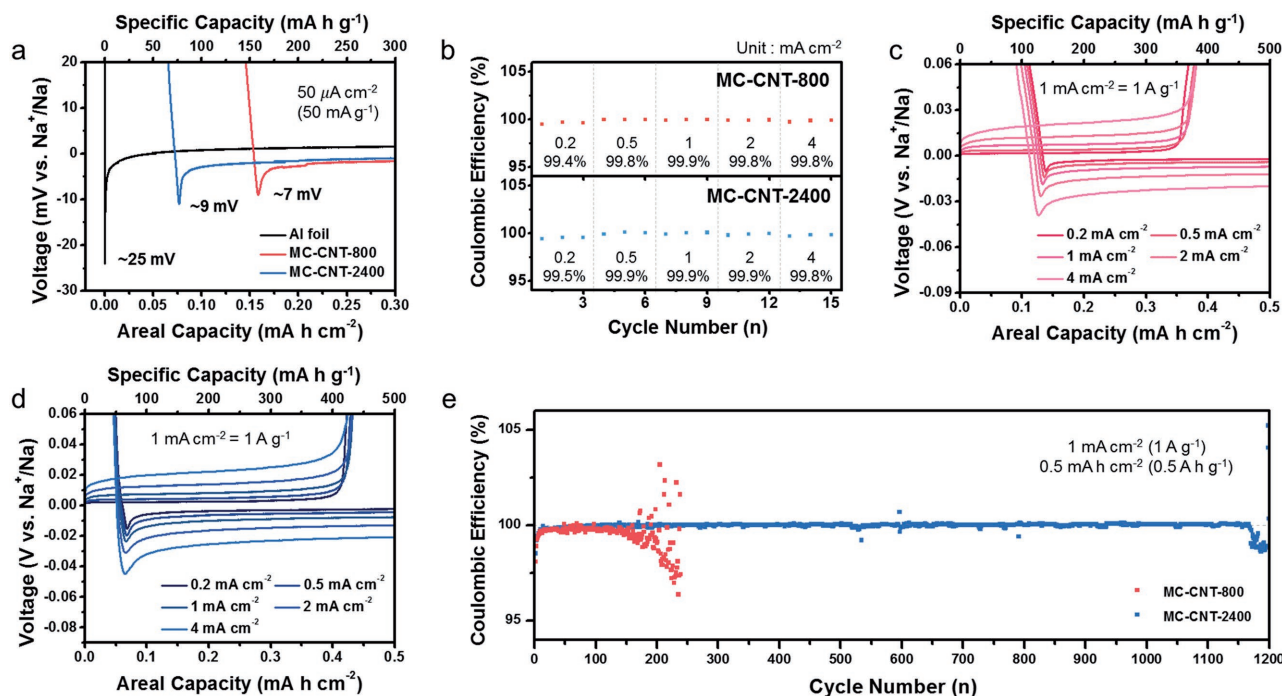


Figure 3. Electrochemical performances of bare Al foil-, MC-CNT-800-, and MC-CNT-2400-based anodes. a) Magnified galvanostatic discharge plots for the 1st cycle at a low current density of $50 \mu\text{A cm}^{-2}$, which shows the various voltage overpotentials of the respective anodes. b) Coulombic efficiencies of MC-CNT-800- and MC-CNT-2400-based anodes by cycle number, characterized at current densities that range from 0.2 to 4 mA cm^{-2} (A g^{-1}). Galvanostatic plating/stripping profiles of c) MC-CNT-800- and d) MC-CNT-2400-based anodes at various current densities from 0.2 to 4 mA cm^{-2} (A g^{-1}). e) Cycling performances of MC-CNT-800- and MC-CNT-2400-based anodes at a current density of 1 mA cm^{-2} with a cut-off capacity of 0.5 mA h cm^{-2} .

that range from 0.2 to 4 mA cm^{-2} . In particular, at 1 mA cm^{-2} (1 A g^{-1}), both electrodes exhibit reasonable Coulombic efficiencies of $\approx 99.9\%$ with stable cycling. In contrast, bare Al foil exhibits a poor Coulombic efficiency of $\approx 93.8\%$, along with significant cell-to-cell variation and cyclical fluctuations, thus demonstrating the usefulness of catalytic carbon templates (Figure S7, Supporting Information). Also, the galvanostatic plating and stripping profiles of MC-CNT-800 and MC-CNT-2400 at various current densities show that the voltage hysteresis increases gradually with the current density (Figure 3c,d). Nevertheless, the voltage hystereses of MC-CNT-800 and MC-CNT-2400 remain within ≈ 50 mV even at a high current density of 4 mA cm^{-2} (4 A g^{-1}). These results clearly contrast to the relatively high voltage hysteresis of the bare Al foil electrode, which reaches 16.7, 30.1, and 61.3 mV at current densities of 1, 2, and 4 mA cm^{-2} , respectively (Figure S8, Supporting Information). The larger MC-CNT active sites can provide additional nucleation sites for Na ion plating, which can induce predominantly homogeneous growth/removal of Na metal, thus suppressing the growth of Na dendrites even at higher current densities. In addition, the DEGDM-based electrolyte is quite stable at the low voltages at which electrolyte degradation and solid-electrolyte interface layer formation is insignificant (Figure S9, Supporting Information). This leads to a high Coulombic efficiency of 99.9% despite the large specific surface areas of the MC-CNT samples. As a result, MC-CNT-2400 exhibits superior cycling stability around 1200 cycles (Figure 3e). This is one of the best cycling performance results reported with a Na metal anode thus far, and indicates a cycle

life several times better than that of MC-CNT-800 (≈ 200 cycles). To investigate the origin of the cycling decay, ex situ XPS analysis was conducted on samples of both MC-CNTs after various numbers of cycles. The C 1s spectra of MC-CNT-800 was measured after 20, 50, 100, and 200 cycles. While carbon sp^3 bonding and C–O/C=O bonding increase continuously, carbon sp^2 bonding decreases, indicating that the aromatic hexagonal carbon structure is damaged by cycling (Figure 4a). In contrast, the C 1s spectra of MC-CNT-2400 indicates that the sp^2 carbon structure is well-maintained even after 1000 cycles, although the conjugated carbon structure deteriorates gradually with cycling (Figure 4b). In addition, ex situ XPS depth profiles indicate the atomic ratios of carbon, oxygen, and sodium in MC-CNT-800 and MC-CNT-2400 after 200 cycles (Figure 4c,d). The depth profile of MC-CNT-800 exhibits a poor carbon content of 20 at% and significant oxygen and Na contents that exceed 70 at%. This result suggests the presence of a large number of residual products after cycling. On the other hand, the major component in the depth profile of MC-CNT-2400 is carbon (≈ 70 at%). Minor oxygen and Na concentrations of <30 at% are observed as well. Ex situ FE-SEM images characterized after 200 cycles show the difference more clearly (Figure S10, Supporting Information). The ex situ FE-SEM image of MC-CNT-800 exhibits a dense morphology distinct from that of pristine MC-CNT-800. This could be due to the presence of moss-like Na compounds and electrolyte decomposition byproducts. In contrast, MC-CNT-2400 preserves its initial morphology after 200 cycles. These ex situ characterizations suggest that the carbon microstructure plays a key role in

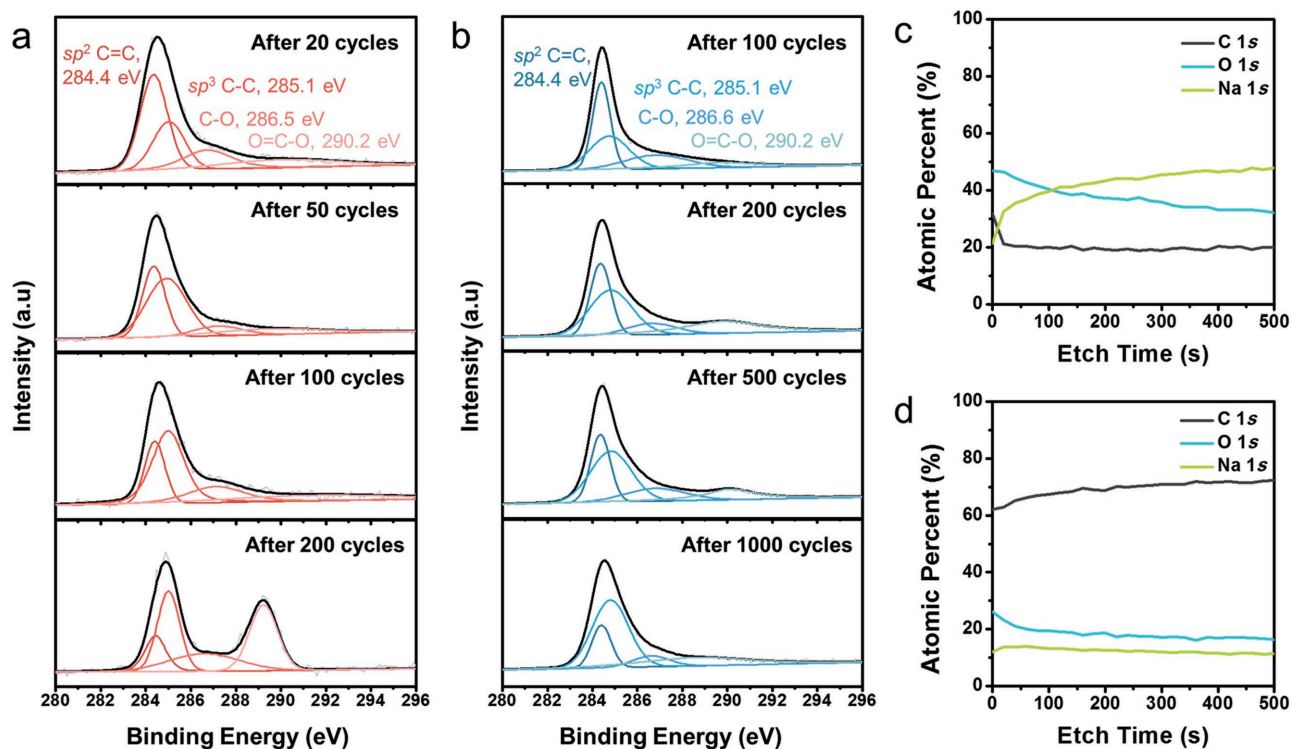


Figure 4. Ex situ XPS analyses of MC-CNT-800 and MC-CNT-2400. Ex situ XPS C 1s spectra of a) MC-CNT-800 (red) and b) MC-CNT-2400 (blue) after various galvanostatic plating/stripping cycles. Ex situ XPS carbon, oxygen, and Na depth profiles of c) MC-CNT-800 and d) MC-CNT-2400 after 200 cycles.

cycling performance via reversible Na metal plating and stripping. The amorphous carbon structure degrades after continuous cycling and finally shuts down after ≈ 200 cycles, while the graphitic structure remains stable over 1000 cycles. The schematic image in Figure S11 of the Supporting Information shows the effects of the carbon microstructure on the cycling stability. An amorphous carbon structure, e.g., MC-CNT-800, is composed of fullerene-like curved and twisted hexagonal carbon structures as its basic structural unit (BSU), due to its large number of topological defects.^[45,52] The negative curvature of the BSU results in a poor stacking order and leads to the formation of numerous closed pores of subnanometer scales in the carbon structure (Figure S11a, Supporting Information).^[53] In contrast, a well-developed graphitic structure, e.g., MC-CNT-2400, has smaller carbon defect sites but larger sp^2 carbon domains than those of amorphous carbons, and has a denser carbon structure (Figure S11b, Supporting Information). The microstructural differences highly affect the cycling stability. Na ions can be inserted into the amorphous carbon structure in an anodic voltage region and stored on the carbon defect sites.^[50,54] When the voltage falls below 0 V, Na metal can be formed on the internal side of the amorphous carbon structure as well as on the top surface (Figure S11c, Supporting Information). As a result, a large interface can be formed between the defective carbon structure and the Na metal, which could accelerate the passivation/degradation of the active carbon surface. In addition, under repetitive cycling, consecutive metal growth/dissolution could lead to a collapse of the randomly aggregated carbon structure. However, the well-developed graphitic struc-

ture has a relatively smaller interface with the Na metal, which could significantly retard the passivation/degradation of the active carbon surface (Figure S11d, Supporting Information). Furthermore, the relatively strong graphitic structure has the ability to endure longer cycles compared with amorphous carbon structures. Hence, both MC-CNT-800 and MC-CNT-2400 have remarkably high Coulombic efficiencies over 150 cycles. However, a significant decay in the Coulombic efficiency could occur for the MC-CNT-800 with a carbon degradation as shown in Figure 3e.

The practicability of MC-CNT-2400 was further demonstrated by a full cell test with its reported cathode counterpart.^[55] As shown in Figure S12a of the Supporting Information, the $Na_{1.5}VPO_{4.8}F_{0.7}$ cathode represents a reversible capacity of ≈ 109 mA h g^{-1} for a voltage range of 2.5–4.4 V versus Na^+/Na at a current rate of 100 mA g^{-1} , for the precycles with the Na metal anode as both the counter and reference electrode. In the full cell system, the galvanostatic charge/discharge profiles for the MC-CNT-2400// $Na_{1.5}VPO_{4.8}F_{0.7}$ device are similar to those of the $Na_{1.5}VPO_{4.8}F_{0.7}$ cathode (Figure S12b, Supporting Information). Moreover, the reversible capacity of the full cell device corresponds to $\approx 84\%$ of that of the $Na_{1.5}VPO_{4.8}F_{0.7}$ cathode. Since the specific weight of MC-CNT-2400 is about 15% of the total electrode weight, the reversible capacity of the full cell device is a reasonable value. Using the profile, the specific energy of the MC-CNT-2400// $Na_{1.5}VPO_{4.8}F_{0.7}$ device was calculated as ≈ 352 Wh kg^{-1} (with an average voltage of 3.82 V), which is a very high value in comparison to previously reported results.^[50,56] In the cycling test, an average Coulombic efficiency of $\approx 99.0\%$ was

achieved during 25 cycles, with the exception of the first cycle, indicating good cycling stability (Figure S12c, Supporting Information). After 25 cycles, a reversible capacity of $\approx 84 \text{ mA h g}^{-1}$ was obtained (Figure S12d, Supporting Information). These results clearly support the feasibility of MC-CNT-2400.

In summary, MC-CNT samples which have the similar macroporous structure but different carbon microstructures were prepared as a Na metal anode, and their electrochemical performances were characterized and compared with them of bare Al foil. While MC-CNT-800 has an amorphous carbon structure with numerous topological carbon defects, MC-CNT-2400 shows a well-developed graphitic structure. The carbon crystallinity of MC-CNT samples played a key role in their electrochemical performances. The defective MC-CNT-800 has more catalytic active sites, showing a lower voltage overpotential value of $\approx 8 \text{ mV}$ at the low current density of $50 \mu\text{A}$ than that of bare Al foil and MC-CNTs-2400. However, in the continuous galvanostatic Na metal plating/stripping process, sp^2 hexagonal carbon structures of MC-CNTs-800 are gradually damaged, exhibiting a dramatic capacity decay at around 200 cycles. In contrast, degradation of the graphitic structure for MC-CNT-2400 is significantly retarded in the repetitive cycles, which cause remarkably improved cycling performances over 1000 cycles with Coulombic efficiency of 99.9%. Moreover, the feasibility of MC-CNT-2400 was demonstrated by full cell tests with a reported $\text{Na}_{1.5}\text{VPO}_{4.8}\text{F}_{0.7}$ cathode, in which an average Coulombic efficiency of $\approx 99.0\%$ was achieved during 25 cycles, with the exception of the first cycle. Hence, the sophisticatedly designed catalytic carbon nanotemplates with a well-developed graphitic structure can be a promising electrode material for Na metal anode.

Experimental Section

Preparation of MC-CNT Samples: Bacterial cellulose (BC) pellicles were produced by *Acetobacter xylinum* BRC 5 in a Hestrin and Schramm medium using a previously reported method.^[57] The solvent from the as-obtained BC hydrogels was exchanged with tert-butanol (99.0%, Sigma-Aldrich, United States), and the hydrogels were freeze-dried at $-45 \text{ }^\circ\text{C}$ and 4.5 Pa for 72 h. The resulting BC cryogels were heated at $5 \text{ }^\circ\text{C min}^{-1}$ to $800 \text{ }^\circ\text{C}$ in a tube furnace under nitrogen flowing at 200 mL min^{-1} , and kept at the target temperature for 2 h. To prepare MC-CNT-2400, MC-CNT-800 was heated at $5 \text{ }^\circ\text{C min}^{-1}$ to $2400 \text{ }^\circ\text{C}$ under Ar using a graphitization furnace (ThermVac, Korea), and kept at the target temperature for 2 h. The as-prepared samples were used without further treatment.

Characterization: Sample morphologies were observed via FE-SEM (S-4300SE, Hitachi, Japan) and FE-TEM (JEM2100F, JEOL, Japan). XRD (Rigaku, DMAX 2500) analyses were conducted using a $\text{Cu K}\alpha$ radiation generator ($\lambda = 0.154 \text{ nm}$) at 40 kV and 100 mA with a 2θ range of 5° – 60° . Raman spectra were measured using a continuous linearly polarized laser with a wavelength of 514.5 nm and a $1200 \text{ groove mm}^{-1}$ grating. The spot diameter of the Raman laser was $\approx 1 \text{ nm}$ with a $100\times$ objective lens. The chemical composition and depth profile were examined using XPS (PHI 5700 ESCA, Chanhassen, USA) with monochromatic Al $\text{K}\alpha$ radiation. The Brunauer–Emmett–Teller specific surface area and differential pore volume were calculated from nitrogen adsorption/desorption isotherms (ASAP 2020, Micromeritics, USA) measured at $-196 \text{ }^\circ\text{C}$.

Electrochemical Characterization: The electrochemical properties of bare Al foil, MC-CNT-800, MC-CNT-2400, and $\text{Na}_{1.5}\text{VPO}_{4.8}\text{F}_{0.7}$ cathode were characterized with the help of a Wonatech automatic battery cycler

and CR2032-type coin cells. For half-cell experiments, coin cells were assembled in a glovebox filled with argon using bare Al foil, MC-CNT-800, MC-CNT-2400, or $\text{Na}_{1.5}\text{VPO}_{4.8}\text{F}_{0.7}$ as the working electrode and metallic Na foil as the reference and counter electrode. NaPF_6 (1 M; Sigma-Aldrich, 98%) was dissolved in a solution of DEGDMC and used as an electrolyte for the Na metal anode. A glass microfiber filter (GF/F, Whatman) was used as a separator. The working electrodes were prepared by mechanically producing MC-CNT-800 or MC-CNT-2400 cylinders $1/2 \text{ in.}$ in diameter. In addition, for the cathode, the working electrodes were prepared by mixing the active material (70 wt%) with conductive carbon (20 wt%) and polyvinylidene fluoride (10 wt%) in *N*-methyl-2-pyrrolidone. The resulting slurries were uniformly applied to the Cu foil. The electrodes were dried at $120 \text{ }^\circ\text{C}$ for 2 h and roll pressed. MC-CNT samples were loaded at densities of $\approx 1 \text{ mg cm}^{-2}$ and galvanostatic discharge/charge cycles were conducted with a capacity limit of 500 mA h cm^{-2} (500 mA h g^{-1}) at various current densities. For the full cell test, the total electrode weight was $\approx 4 \text{ mg}$, and the weight ratio of MC-CNT-2400 was $\approx 15\%$.

Supporting Information

Supporting Information is available from the Wiley Online Library or from the author.

Acknowledgements

This research was supported by the Basic Science Research Program through the National Research Foundation of Korea (NRF) funded by the Ministry of Education (NRF-2016R1A2B4009601) and (NRF-2017R1C1B1004167). This work was also supported by Industrial Strategic Technology Development Program, (Project No. 10050477, Development of separator with low thermal shrinkage and electrolyte with high ionic conductivity for Na-ion batteries) funded by the Ministry of Trade, Industry & Energy (MI, Korea).

Conflict of Interest

The authors declare no conflict of interest.

Keywords

carbon nanofibers, carbon template, macroporous carbon, metal anode, sodium ion batteries

Received: May 9, 2017

Revised: July 20, 2017

Published online: November 7, 2017

- [1] M. Armand, J.-M. Tarascon, *Nature* **2008**, *451*, 652.
- [2] V. Etacheri, R. Marom, R. Elazari, G. Salitra, D. Aurbach, *Energy Environ. Sci.* **2011**, *4*, 3243.
- [3] D. Larcher, J.-M. Tarascon, *Nat. Chem.* **2015**, *7*, 19.
- [4] T.-H. Kim, J.-S. Park, S. K. Chang, S. Choi, J. H. Ryu, H.-K. Song, *Adv. Energy Mater.* **2012**, *2*, 860.
- [5] J. B. Goodenough, K.-S. Park, *J. Am. Chem. Soc.* **2013**, *135*, 1167.
- [6] L. Luo, J. Wu, J. Xu, V. P. Dravid, *ACS Nano* **2014**, *8*, 11560.
- [7] L. Li, R. Jacobs, P. Gao, L. Gan, F. Wang, D. Morgan, S. Jin, *J. Am. Chem. Soc.* **2016**, *138*, 2838.
- [8] J. Mujtaba, H. Sun, G. Huang, K. Mølhave, Y. Liu, Y. Zhao, X. Wang, S. Xu, J. Zhu, *Sci. Rep.* **2016**, *6*, 20592.

- [9] B. Wang, X. Li, X. Zhang, B. Luo, M. Jin, M. Liang, S. A. Dayeh, S. T. Picraux, L. Zhi, *ACS Nano* **2013**, *7*, 1437.
- [10] H. Tao, L.-Z. Fan, W.-L. Song, M. Wu, X. He, X. Qu, *Nanoscale* **2014**, *6*, 3138.
- [11] C. Wu, Y. Jiang, P. Kopold, P. A. van Aken, J. Maier, Y. Yu, *Adv. Mater.* **2016**, *28*, 7276.
- [12] Y. Zheng, T. Zhou, C. Zhang, J. Mao, H. Liu, Z. Guo, *Angew. Chem., Int. Ed.* **2016**, *55*, 3408.
- [13] J. W. Wang, X. H. Liu, S. X. Mao, J. Y. Huang, *Nano Lett.* **2012**, *12*, 5897.
- [14] Y. Liu, N. Zhang, L. Jiao, Z. Tao, J. Chen, *Adv. Funct. Mater.* **2015**, *25*, 214.
- [15] J.-G. Zhang, W. Xu, W. A. Herderson, *Lithium Metal Anodes and Rechargeable Lithium Metal Batteries*, Springer International Publishing, Switzerland **2017**.
- [16] H. Kim, G. Jeong, Y.-U. Kim, J.-H. Kim, C.-M. Park, H.-J. Sohn, *Chem. Soc. Rev.* **2013**, *42*, 9011.
- [17] W. Xu, J. Wang, F. Ding, X. Chen, E. Nasybulin, Y. Zhang, J.-G. Zhang, *Energy Environ. Sci.* **2014**, *7*, 513.
- [18] K. J. Harry, D. T. Hallinan, D. Y. Parkinson, A. A. MacDowell, N. P. Balsara, *Nat. Mater.* **2014**, *13*, 69.
- [19] Y. Liu, D. Lin, Z. Liang, J. Zhao, K. Yan, Y. Cui, *Nat. Commun.* **2016**, *7*, 10992.
- [20] Z. Liang, D. Lin, J. Zhao, Z. Lu, Y. Liu, C. Liu, Y. Lu, H. Wang, K. Yan, X. Tao, Y. Cui, *Proc. Natl. Acad. Sci. USA* **2016**, *113*, 2862.
- [21] J. Steiger, D. Kramer, R. Mönig, *J. Power Sources* **2014**, *261*, 112.
- [22] D. Lu, Y. Shao, T. Lozano, W. D. Bennett, G. L. Graff, B. Polzin, J. Zhang, M. H. Engelhard, N. T. Saenz, W. A. Henderson, P. Bhattacharya, J. Liu, J. Xiao, *Adv. Energy Mater.* **2015**, *5*, 1400993.
- [23] X.-B. Cheng, T.-Z. Hou, R. Zhang, H.-J. Peng, C.-Z. Zhao, J.-Q. Huang, Q. Zhang, *Adv. Mater.* **2016**, *28*, 2888.
- [24] F. Ding, W. Xu, G. L. Graff, J. Zhang, M. L. Sushko, X. Chen, Y. Shao, M. H. Engelhard, Z. Nie, J. Xiao, X. Liu, P. V. Sushko, J. Liu, J.-G. Zhang, *J. Am. Chem. Soc.* **2013**, *135*, 4450.
- [25] W. Li, H. Yao, K. Yan, G. Zheng, Z. Liang, Y.-M. Chiang, Y. Cui, *Nat. Commun.* **2015**, *6*, 7436.
- [26] F. Ding, W. Xu, X. Chen, J. Zhang, M. H. Engelhard, Y. Zhang, B. R. Johnson, J. V. Crum, T. A. Blake, X. Liu, J.-G. Zhang, *J. Electrochem. Soc.* **2013**, *160*, A1894.
- [27] Y. Lu, Z. Tu, L. A. Archer, *Nat. Mater.* **2014**, *13*, 961.
- [28] R. Miao, J. Yang, X. Feng, H. Jia, J. Wang, Y. Nuli, *J. Power Sources* **2014**, *271*, 291.
- [29] Y. Zhang, J. Qian, W. Xu, S. M. Russell, X. Chen, E. Nasybulin, P. Bhattacharya, M. H. Engelhard, D. Mei, R. Cao, F. Ding, A. V. Cresce, K. Xu, J.-G. Zhang, *Nano Lett.* **2014**, *14*, 6889.
- [30] C. Zu, N. Azimi, Z. Zhang, A. Manthiram, *J. Mater. Chem. A* **2015**, *3*, 14864.
- [31] D. Lin, Y. Liu, Z. Liang, H.-W. Lee, J. Sun, H. Wang, K. Yan, J. Xie, Y. Cui, *Nat. Nanotechnol.* **2016**, *11*, 626.
- [32] A. Zhang, X. Fang, C. Shen, Y. Liu, C. Zhou, *Nano Res.* **2016**, *9*, 3428.
- [33] A. P. Cohn, N. Muralidharan, R. Carter, K. Share, C. L. Pint, *Nano Lett.* **2017**, *17*, 1296.
- [34] G. Zheng, S. W. Lee, Z. Liang, H.-W. Lee, K. Yan, H. Yao, H. Wang, W. Li, S. Chu, Y. Cui, *Nat. Nanotechnol.* **2014**, *9*, 618.
- [35] Y. Zhang, W. Luo, C. Wang, Y. Li, C. Chen, J. Song, J. Dai, E. M. Hitz, S. Xu, C. Yang, Y. Wang, L. Hu, *Proc. Natl. Acad. Sci. USA* **2017**, *114*, 3584.
- [36] K. Xie, W. Wei, K. Yuan, W. Lu, M. Guo, Z. Li, Q. Song, X. Liu, J.-G. Wang, C. Shen, *ACS Appl. Mater. Interfaces* **2016**, *8*, 26091.
- [37] E. Kazyak, K. N. Wood, N. P. Dasgupta, *Chem. Mater.* **2015**, *27*, 6457.
- [38] Y. Zhao, L. V. Goncharova, A. Lushington, Q. Sun, H. Yadegari, B. Wang, W. Xiao, R. Li, X. Sun, *Adv. Mater.* **2017**, *29*, 1606663.
- [39] N.-W. Li, Y.-X. Yin, C.-P. Yang, Y.-G. Guo, *Adv. Mater.* **2016**, *28*, 1853.
- [40] Y.-J. Kim, H. Lee, H. Noh, J. Lee, S. Kim, M.-H. Ryou, Y. M. Lee, H.-T. Kim, *ACS Appl. Mater. Interfaces* **2017**, *9*, 6000.
- [41] R. Miao, J. Yang, Z. Xu, J. Wang, Y. Nuli, L. Sun, *Sci. Rep.* **2016**, *6*, 21771.
- [42] J. Qian, W. A. Henderson, W. Xu, P. Bhattacharya, M. Engelhard, O. Borodin, J.-G. Zhang, *Nat. Commun.* **2015**, *6*, 6362.
- [43] Z. W. Seh, J. Sun, Y. Sun, Y. Cui, *ACS Cent. Sci.* **2015**, *1*, 449.
- [44] R. Cao, K. Mishra, X. Li, J. Qian, M. H. Engelhard, M. E. Bowden, K. S. Han, K. T. Mueller, W. A. Henderson, J.-G. Zhang, *Nano Energy* **2016**, *30*, 825.
- [45] S. Y. Cho, Y. S. Yun, S. Lee, D. Jang, K.-Y. Park, J. K. Kim, B. H. Kim, K. Kang, D. L. Kaplan, H.-J. Jin, *Nat. Commun.* **2015**, *6*, 7145.
- [46] M. Y. Song, N. R. Kim, H. J. Yoon, S. Y. Cho, H.-J. Jin, Y. S. Yun, *ACS Appl. Mater. Interfaces* **2017**, *9*, 2267.
- [47] M. Y. Song, N. R. Kim, S. Y. Cho, H.-J. Jin, Y. S. Yun, *ACS Sustainable Chem. Eng.* **2017**, *5*, 616.
- [48] N. R. Kim, Y. S. Yun, M. Y. Song, S. J. Hong, M. Kang, C. Leal, Y. W. Park, H.-J. Jin, *ACS Appl. Mater. Interfaces* **2016**, *8*, 3175.
- [49] K. Yan, Z. Lu, H.-W. Lee, F. Xiong, P.-C. Hsu, Y. Li, J. Zhao, S. Chu, Y. Cui, *Nat. Energy* **2016**, *1*, 16010.
- [50] Y. S. Yun, K.-Y. Park, B. Lee, S. Y. Cho, Y.-U. Park, S. J. Hong, B. H. Kim, H. Gwon, H. Kim, S. Lee, Y. W. Park, H.-J. Jin, K. Kang, *Adv. Mater.* **2015**, *27*, 6914.
- [51] Y. S. Yun, D.-H. Kim, S. J. Hong, M. H. Park, Y. W. Park, B. H. Kim, H.-J. Jin, K. Kang, *Nanoscale* **2015**, *7*, 15051.
- [52] P. J. F. Harris, A. Burian, S. Duber, *Philos. Mag. Lett.* **2000**, *80*, 381.
- [53] Y. S. Yun, S. Lee, N. R. Kim, M. Kang, C. Leal, K.-Y. Park, K. Kang, H.-J. Jin, *J. Power Sources* **2016**, *313*, 142.
- [54] D. Datta, J. Li, V. B. Shenoy, *ACS Appl. Mater. Interfaces* **2014**, *6*, 1788.
- [55] Y.-U. Park, D.-H. Seo, H.-S. Kwon, B. Kim, J. Kim, H. Kim, I. Kim, H.-I. Yoo, K. Kang, *J. Am. Chem. Soc.* **2013**, *135*, 13870.
- [56] Z. Chen, V. Augustyn, X. Jia, Q. Xiao, B. Dunn, Y. Lu, *ACS Nano* **2012**, *6*, 4319.
- [57] Y. S. Yun, H. Bak, H.-J. Jin, *Synth. Met.* **2010**, *160*, 561.